e-ISSN: 2550-164X

Available online at
https://jmeche.uitm.edu.my/browse-journals/regular-issue/regular-issue-2025-vol-22-3/

Journal of Mechanical Engineering 22(3) 2025, 196 – 208.

Journal of Mechanical Engineering

Influence of Trip Wires on Turbulence and Vorticity for a Cylinder Bluff Body

Mohd Hafiz Mohd Noh[1*], Ahmad Hussein Abdul Hamid[1], Mohd Ridzuan Sejon[1], Waseem Ahmed Rzaij Faraj[1]

[1]*Faculty of Mechanical Engineering, Universiti Teknologi MARA, 40450, Shah Alam, Malaysia*

ARTICLE INFO

Article history:
Received 01 December 2024
Revised 25 August 2025
Accepted 26 August 2025
Online first
Published 15 September 2025

Keywords:
Cylinder bluff body
Tripwire angles
Heat transfer
Vorticity
Velocity

DOI:
https://doi.org/10.24191/jmeche.v22i3.3613

ABSTRACT

Bluff bodies have been extensively studied across various industries, including aerospace, civil, mechanical, and offshore engineering, owing to their widespread applications. This study focuses on enhancing heat transfer from duct walls by inducing intense flow vorticity downstream of cylindrical bluff bodies. Trip wires are employed on these bodies, arranged in an infinite array, with wire angles ranging from 45° to 135°, within a cooling duct. The objective is to investigate the impact of turbulence enhancement on heat transfer performance, wake formation, and vorticity behavior in a flow channel featuring an infinite array configuration. OpenFoam software has been used to solve governing equations with prescribed boundary conditions, followed by post-processing the data in Paraview and Octave software. Observations reveal that trip wires significantly modify flow transition and wake development downstream of the bluff body, resulting in enhanced turbulence within the channel. Trip wires positioned at a separation angle of 85° have a pronounced effect on the evolution of turbulent flow in the wake region, promoting greater flow mixing, which accelerates convective heat transfer along the streamwise direction and improves the local Nusselt number on the wall surface. The shedding frequency analysis shows the highest peak occurring at the 85° separation angle. Overall, the numerical results highlight the influence of heat transfer generation in relation to all variables examined in this study

INTRODUCTION

Extensive research has been conducted on the study of flow behavior, specifically in laminar and turbulent states, with a particular focus on wake formation due to its important engineering application such as heat exchangers, concerning electronic industries, nuclear reactors, and refrigeration systems. These investigations have been approached from both experimental and numerical perspectives. In practical applications, phenomena such as vortex shedding and separation during flow transition cannot be

[1*] Corresponding author. *E-mail address*: hafiz66@uitm.edu.my
https://doi.org/10.24191/jmeche.v22i3.3613

disregarded due to their significant impact on the flow's erratic nature (Roshko, 1955). Wake formation refers to the disturbed flow region that typically occurs downstream of a solid body, where fluid flows around the object in a turbulent manner. Bluff bodies, specifically cylinder shapes, have been extensively utilized to study wake formation. Cylinder bluff bodies have garnered substantial attention due to their versatile applications, including vortex flow meters, heat exchange systems, and micro mixers (Dhiman & Shyam, 2011). Moreover, the appropriate shape and dimensions of bluff bodies are crucial, as they can significantly influence the deviation and reduction of flow or heat transfer from desired values.

Previous investigations have utilized the Rhombus Cylinder as a bluff body to guide the transition from laminar to turbulent flow. These studies revealed that the presence of the Rhombus Cylinder led to an increase in efficiency beyond unity, primarily due to enhanced heat transfer. The effect of the Rhombus Cylinder on heat transfer was more prominent than the effects resulting from increased friction, and vice versa (Bhattacharyya et al., 2017). Sahin et al. (2013) examined overall heat transfer enhancement using triangular obstacles. The researchers observed that the presence of equilateral triangular obstacles in the flow field promoted greater flow mixing, facilitating heat transfer processes. The position of the triangles and the Reynolds number significantly affected the temperature distribution behind the bluff bodies, causing notable changes in the vertical direction along the targeted distance. Behara & Mittal (2011) investigated the effect of a trip on a circular cylinder with the purpose to promotes the transition of the boundary layer. The study found that the existence of a trip causes the upper surface of the boundary layer to change to a turbulent state with a low Reynolds number, resulting in a rapid decrease in drag and the first stage of the drag crisis.

Murmu et al. (2020) showed the influence of turbulent intensity on the flow behavior around two-dimensional bluff bodies using numerical simulations. Different bluff bodies, such as triangular prism, diamond, and trapezoidal, are taken into attention. The analysis covers turbulent and laminar regimes with Reynolds numbers ranging up to 200,000 and inlet intensities between 5% and 40%. The study highlights the transition SST Model's effectiveness in calculating heat transfer for both laminar and turbulent flows, as well as the importance of the inlet turbulent intensity's considerable impact on the drag coefficient. Vyas et al. (2020) experimentally studied the flow and heat transfer characteristics in the wake region of a semi-circular cylinder embedded within a rectangular channel were investigated using non-intrusive techniques. The semi-circular cylinder, with a blockage ratio of 0.45 (d/H), created a wake region downstream by obstructing the incoming totally improved laminar flow. The velocity field in the wake region was analyzed using particle image velocimetry (PIV) with water as the working medium. The interactions between the fluctuating shear layers, vortices shed by the cylinder, and the heated bottom wall of the channel were observed.

The influence of the cylinder's wake region on heat transfer was examined, and the overall heat transfer characteristics were found to be improved passively. Interferometry was employed to measure the whole field temperature values, and the heat transfer rates were compared with those of a plain channel without a cylinder. The Schlieren technique was used to identify the dominant frequencies of the unsteady flow downstream of the cylinder. The presence of the semi-circular cylinder in the channel resulted in a heat transfer enhancement of up to 42% compared to the flow in a plain channel for the Reynolds number range of 75 - 200, which was the scope of the experiments. Luo et al. (2021) examined the flow properties and heat transfer mechanism when fluid flows through an oscillating cylinder using a numerical simulation. The research takes into account various Reynolds numbers (Re = 197,248,296) with changes in oscillation amplitude, frequency, and angle. The outcomes reveal that magnitude has a large influence upon the flow field, but frequency has a smaller impact. Heat transmission is often improved by increasing amplitude and frequency.

https://doi.org/10.24191/jmeche.v22i3.3613

The field synergy approach is used to investigate the process behind heat transfer enhancement. For changing oscillating angles, the flow field displays multiple regimes, and the Nusselt number originally declines and subsequently increases. The optimized angle is typically observed at 0° or 90° in most cases. The studies applied an immersed boundary method to facilitate the placement of the cylinder within the Cartesian grid system, which concluded that flow topology significantly changes depending upon the gap, resulting in the related change of instability characteristics (Lee & Yang, 2013). Despite numerous efforts that have been performed on the study of wake formation behavior using bluff bodies, lesser consideration has been given to the implementation of an infinite array arrangement of cylinder bluff bodies, particularly on turbulence enhancement of flow. The present investigation seeks to address this gap with the help of numerical simulations.

In multiphase systems, heat transmission between a sphere and its surrounding fluid is a critical issue. While extensive research has been conducted on external and internal heat transfer problems, conjugate problems have received comparatively less attention. Recent advancements in computational power and modeling techniques have made numerical simulations a valuable tool for gaining deeper insights into these phenomena. To simulate conjugate heat transfer, many ways have been presented, which may be classified as the Lattice Boltzmann Method (LBM) approach (Konopliv & Sparrow, 1970; Abramzon & Elata, 1984), the Stokes analytical method (Nguyen et al., 1993; Romkes et al., 2003) and the Navier-Stokes method (Kravets et al., 2019; Chambré & Young, 1958), all of which are based on the manipulation of the fluid surrounding the sphere.

The demand for high thermal system performance has prompted researchers to employ several heat transfer optimization strategies. Conventional techniques of lowering thermal resistance include expanding the surface area of the heat exchanger or decreasing the thickness of the thermal boundary layer on the heat exchanger's surface. Nevertheless, increasing the surface area also results in a raise in the heat exchanger's mass or volume, as well as the cost of the materials. The creation of vortices is one technique for reducing the thickness of the boundary layer (Kravets et al., 2019). Heat transfer augmentation techniques are classified into three types: active methods that require external power such as mechanical aids, surface vibration, fluid vibration, and electrostatic fields, passive methods that do not require direct external power such as rough surfaces, extended surfaces, displaced promoters, vortex flow devices, and fluid additives, and hybrid methods that combine both active and passive methods.

The flow study over a bluff body has been actively being study recently. Duan et al. (2021) has investigated the effects of leading-edge separation on the vibration of an elongated bluff body, found that by placing a splitter plate in the wake of the mode, the interaction between the upper- and lower layer flow is prevented. Using trip wire as passive flow control on a sphere can reduced velocities ($U* > 10$) with a maximum reduction of up to 97%, and the influence of trip wire location and diameter ratio can lead for altering the main flow separation location, which will greatly influence the wake flow of the cylinder bluff body (Sareen et al., 2024). The influence of trip wire location and height on aerodynamic performance also being investigated, and indicated that at optimal configurations, both trip configurations delay the final flow separation, leading to a pronounced drag crisis, a sharp drop in drag coefficient (Chopra & Mittal, 2022). Research by Lysenko et al. (2023) utilized large eddy simulations (LES) to analyze the effect of active flow control for the wake flow of a bluff body. They found that two trapped vortex cells implemented at the upper side successfully control the behavior of boundary layers, demonstrating almost detached flow and suppressing the vortex street with 10% of the drag reduction. In order to reduce the computational time and cost, recent advances from the machine learning approach can be adopted to predict the flow characteristics and hydrodynamic responses of the cylinders with different geometries (Lekkala et al., 2022).

https://doi.org/10.24191/jmeche.v22i3.3613

METHODOLOGY

For an incompressible flow, the conservation of mass of Newtonian Isothermal equations in three dimensions is represented as follows:

$$\nabla.\nu = \frac{1}{r}\frac{\partial r(\nu_r)}{\partial r} + \frac{1}{\theta}\frac{\partial(\nu_\theta)}{\partial\theta} + \frac{\partial(\nu_z)}{\partial z} = 0 \tag{1}$$

The conservation of momentum is given as follows:

$$\rho\frac{\partial \nu}{\partial t} = \mu\nabla^2\nu - \rho(\nu.\nabla)\nu - \nabla.\rho \tag{2}$$

In component form: *r*, *θ,* and *z* directions that are respectively given by: -

$$\begin{aligned}&\frac{\partial \nu_r}{\partial t} + \nu_r\frac{\partial \nu_r}{\partial r} + \frac{\nu_\theta}{r}\frac{\partial(\nu_r)}{\partial\theta} + \nu_z\frac{\partial \nu_r}{\partial z} - \frac{\nu_\theta^2}{r} = -\frac{1}{\rho}\frac{\partial p}{\partial r}\\ &+\frac{\mu}{\rho}\left[\frac{1}{r}\frac{\partial}{\partial r}\left(r\frac{\partial \nu_r}{\partial r}\right) + \frac{1}{r^2}\left(\frac{\partial^2\nu_r}{\partial\theta^2}\right) + \frac{\partial^2\nu_r}{\partial z^2} + \frac{2}{r^2}\left(\frac{\partial \nu_\theta}{\partial\theta}\right) + \frac{\nu_r}{r^2}\right]\end{aligned} \tag{3}$$

$$\begin{aligned}&\frac{\partial \nu_\theta}{\partial t} + \nu_r\frac{\partial \nu_\theta}{\partial r} + \frac{\nu_\theta}{r}\frac{\partial(\nu_\theta)}{\partial\theta} + \nu_z\frac{\partial \nu_\theta}{\partial z} - \frac{\nu_r\nu_\theta}{r} = -\frac{1}{\rho}\frac{1}{r}\frac{\partial p}{\partial\theta}\\ &+\frac{\mu}{\rho}\left[\frac{1}{r}\frac{\partial}{\partial r}\left(r\frac{\partial \nu_\theta}{\partial r}\right) + \frac{1}{r^2}\left(\frac{\partial^2\nu_r}{\partial\theta^2}\right) + \frac{\partial^2\nu_\theta}{\partial z^2} + \frac{2}{r^2}\left(\frac{\partial \nu_r}{\partial\theta}\right) + \frac{\nu_\theta}{r^2}\right]\end{aligned} \tag{4}$$

$$\frac{\partial \nu_z}{\partial t} + \nu_r\frac{\partial \nu_z}{\partial r} + \frac{\nu_\theta}{r}\frac{\partial(\nu_z)}{\partial\theta} + \nu_z\frac{\partial \nu_z}{\partial z} = -\frac{1}{\rho}\frac{\partial p}{\partial z} + \frac{\mu}{\rho}\left[\frac{1}{r}\frac{\partial}{\partial r}\left(r\frac{\partial \nu_z}{\partial r}\right) + \frac{1}{r^2}\left(\frac{\partial^2\nu_z}{\partial\theta^2}\right) + \frac{\partial^2\nu_z}{\partial z^2}\right] \tag{5}$$

where *v*, *ρ*, *p*, and *μ* are the velocity, density, pressure, and viscosity of the fluid. Implemented non-dimensionalization into the system, hence the modified term will become:

$$\begin{aligned}&\frac{\partial \nu_r}{\partial t} + \nu_r\frac{\partial \nu_r}{\partial r} + \frac{\nu_\theta}{r}\frac{\partial(\nu_r)}{\partial\theta} + \nu_z\frac{\partial \nu_r}{\partial z} - \frac{\nu_\theta^2}{r} = -\frac{1}{Re}\frac{\partial p}{\partial r}\\ &+\frac{\mu}{Re}\left[\frac{1}{r}\frac{\partial}{\partial r}\left(r\frac{\partial \nu_r}{\partial r}\right) + \frac{1}{r^2}\left(\frac{\partial^2\nu_r}{\partial\theta^2}\right) + \frac{\partial^2\nu_r}{\partial z^2} + \frac{2}{r^2}\left(\frac{\partial \nu_\theta}{\partial\theta}\right) + \frac{\nu_r}{r^2}\right]\end{aligned} \tag{6}$$

$$\begin{aligned}&\frac{\partial \nu_\theta}{\partial t} + \nu_r\frac{\partial \nu_\theta}{\partial r} + \frac{\nu_\theta}{r}\frac{\partial(\nu_\theta)}{\partial\theta} + \nu_z\frac{\partial \nu_\theta}{\partial z} - \frac{\nu_r\nu_\theta}{r} = -\frac{1}{Re}\frac{1}{r}\frac{\partial p}{\partial\theta}\\ &+\frac{\mu}{Re}\left[\frac{1}{r}\frac{\partial}{\partial r}\left(r\frac{\partial \nu_\theta}{\partial r}\right) + \frac{1}{r^2}\left(\frac{\partial^2\nu_r}{\partial\theta^2}\right) + \frac{\partial^2\nu_\theta}{\partial z^2} + \frac{2}{r^2}\left(\frac{\partial \nu_r}{\partial\theta}\right) + \frac{\nu_\theta}{r^2}\right]\end{aligned} \tag{7}$$

$$\frac{\partial \nu_z}{\partial t} + \nu_r\frac{\partial \nu_z}{\partial r} + \frac{\nu_\theta}{r}\frac{\partial(\nu_z)}{\partial\theta} + \nu_z\frac{\partial \nu_z}{\partial z} = -\frac{1}{Re}\frac{\partial p}{\partial z} + \frac{\mu}{Re}\left[\frac{1}{r}\frac{\partial}{\partial r}\left(r\frac{\partial \nu_z}{\partial r}\right) + \frac{1}{r^2}\left(\frac{\partial^2\nu_z}{\partial\theta^2}\right) + \frac{\partial^2\nu_z}{\partial z^2}\right] \tag{8}$$

where *Re* is Reynolds Number in function of characteristic velocity, V_∞ , and characteristic length, *L* which can be expressed by:

https://doi.org/10.24191/jmeche.v22i3.3613

$$\mathrm{Re} = \frac{\rho V_\infty L}{\mu} \tag{9}$$

The flow configuration and geometry used in this study are depicted in Fig 1. The internal flow of the fluid occurs in a left-to-right direction, following an infinite array arrangement that repeats periodically in both directions. To study the effects of the trip wire, cylindrical objects with a diameter, d, are placed at the upper and lower circumferential positions of the main cylinder. Each case is assigned a specific range of angles for the trip wire. In the trip wire case, a Reynolds number (*Re*) of 120 is imposed, and a constant mass flow rate is maintained at the inlet of the duct. This ensures a constant flow of fluid passing through the bluff body. To ensure that the flow is fully developed in the channel, the distances of the inlet and outlet boundaries from the main cylinder are denoted as *L* and 3*L*, respectively. This arrangement ensures that the solution is independent of the domain size, and a no-slip condition is imposed at both the channel and cylinder walls. The fluid flow is considered to be Newtonian and incompressible. The thermophysical properties of the nanofluid formulation are influenced by the buoyancy force and are modelled using the Boussinesq approximation.

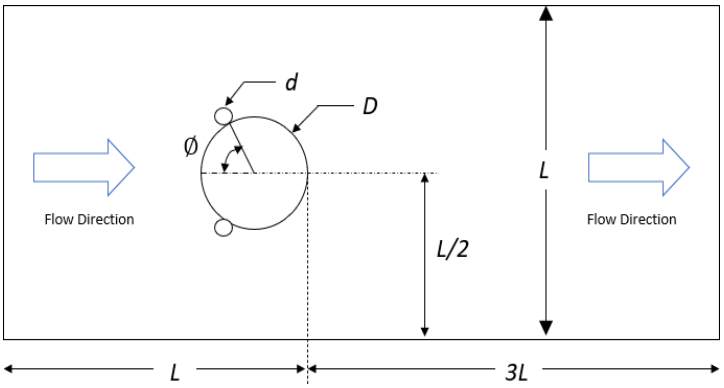

Fig. 1. Schematic representation of numerical domain. The arrow indicates the direction of flow.

The periodic boundary condition is applied at the inlet and outlet for this calculation. The volume flow rate has been specified at the inlet, and the velocity profile at the outlet will fuel to the inlet. The non-slip boundary condition at both the channel and cylinder wall ($u = v = w = 0$). In this study, the open-source computational fluid dynamics (CFD) framework OpenFOAM was utilized. The governing equations, along with their corresponding boundary conditions, were solved using the finite volume method (FVM). To solve the flow field, the SIMPLE algorithm was employed. A second-order upwind differencing technique was utilized for the convection terms. The flow is incompressible, and a laminar low Reynolds number is considered. This scheme is known for its accuracy in handling convection-dominated flows. Additionally, the second-order upwind differencing scheme was used to handle the diffusion terms in the momentum and energy equations. To capture the velocity gradient accurately, the grid was refined in the vicinity of the cylinder and around 0.75*L* downstream distance from the cylinder bluff body. This refinement ensured a more precise representation of the flow characteristics in those areas. A grid independence study was conducted using four different cell counts. Fig 2 illustrates the drag coefficient error percentage for each configuration, indicating that the grid size of 140,000 exhibits the lowest error compared to the others. During the CFD simulation, the scaled residual values for the energy and velocity components were set to 10-9. This criterion ensures that the solution achieves a high level of convergence and accuracy.

https://doi.org/10.24191/jmeche.v22i3.3613

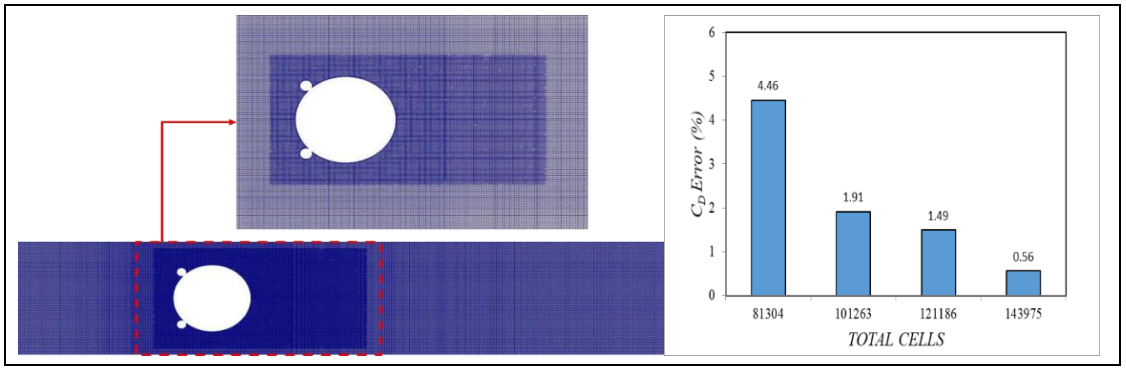

Fig. 2. Domain meshing of the flow channel, the finer meshing around the cylinder body and grid independence study.

The numerical domain consists of cylinder bluff bodies with the presence of trip wires on the circumferential area of the bluff body. The circular cylinder body with a diameter D, is positioned at the centerline of the channel flow and separated by the parameter distance of the duct wall channel. The presence of a trip wire with diameter d, is placed at the upper and lower circumferential of the main cylinder based on the range of angles assigned to each case. The computational domain was divided into a number of elements, and appropriate boundary conditions were applied to solve the governing equations. The mesh was refined near the cylinder and approximately $0.75L$ downstream from the bluff body, as shown in Fig 2. This refinement ensured the accuracy of the solutions by capturing the flow characteristics in those regions.

RESULTS AND DISCUSSION

The flow of fluid over cylindrical bluff bodies with the inclusion of trip wires in an infinite array has been numerically simulated. The flow was adjusting to a constant Reynolds number of 120 while the location of the trip wires was changed with a separation angle between 45° and 135°, symmetrically located about the stagnation point and at the circumferential area of the cylinder bluff bodies. This result was accomplished by using OpenFoam software to solve the governing equations with specified boundary conditions, and the data was then post-processed in Paraview and Octave software. The findings presented in Lee & Yang (2013) are utilized to validate the numerical solver employed in the current study. The graphic in Fig 3 that contrasts the data from the current simulation with previously published data highlights the time-averaged drag coefficient, which is the data of particular importance. The Reynolds number ranges from $Re = 120$ to $Re = 155$.

The data shown by Lee & Yang (2013) is based on the flow instability in an obstructed channel, whereby the data is numerically studied using an arrangement of an infinite array of equi-spaced circular cylinders, which is practically the same type of arrangement as the present study, with the main differences is the type of bluff bodies applied in the flow channel arrangement. According to the plotted data, the average drag coefficient of the current mesh data essentially follows the same pattern as that of the previous study by Lee & Yang (2013), which showed that variations in the type of arrangement and variables used in the flow channel had a slightly lesser impact on the average drag coefficient. Nevertheless, there is some variation in the patterns of the average drag coefficient, which is mostly caused by the unstable shear layer separation that occurs when the Reynolds number is increased. The deviation range value between the simulation result and the reference is 0.002.

https://doi.org/10.24191/jmeche.v22i3.3613

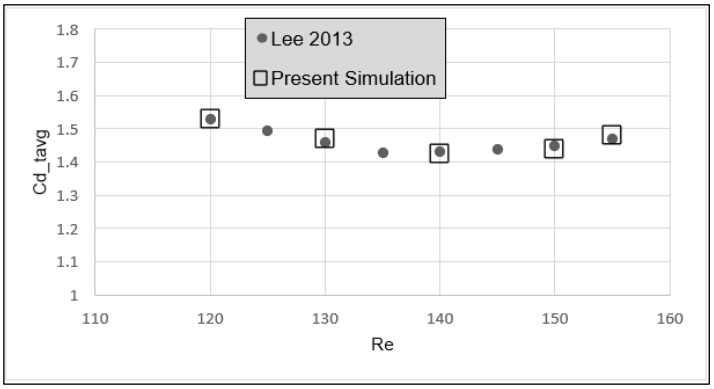

Fig. 3. Validation of average drag coefficient versus Reynolds Number.

Vorticity Flow Field

Fig 4 depicts the vorticity contour plots of the flow field as it passes past cylindrical bluff bodies. Fig 4(a), which depicts the flow through a cylinder's bluff body without a trip wire, demonstrates that there are variations and developments in the flow past the cylinder, although they are less apparent when a trip wire is used. That is, using trip wire leads to greater variation and improvement, which causes vortex to shed vigorously behind the bluff body, resulting in enhanced turbulent flow. Figs 4(b) to 4(e) depict unstable vortex shedding, which occurs as a result of the angle of the trip wires and promotes significant variations in the flow behind the bluff bodies.

The phenomenon corresponds with Behara and Mithal's hypothesis on the influence of the trip wire on flow, which states that the presence of a trip on the cylinder's bluff body causes an early transition of the boundary layer (Behara & Mittal, 2011). As a result, even if the Reynolds number is constant in all circumstances, the flow practically attains different states of flow on the upper and lower edges in many of the flow regimes. As the separation angles applied to the cylinder bluff body increase, the strength of vortex shedding increases, which aggressively forms behind the bluff body. Based on Fig 4(b), the intensity of vortex shedding to occur is relatively less vigorous compared with the higher separation angle, as shown in Fig 4(d) and Fig 4(e). The position of the separation angle, which is nearly behind the cylinder bluff body, significantly promotes faster formation of vortex shedding with the near stretch of shear layer downstream of the flow in the vicinity of the cylinder, as shown in Fig 4(d).

Additionally, the vortex shedding condition shows a significant difference in shedding intensity at the separation angle of 85°, as shown in Fig 4(c), owing to the position of the separation angles being almost parallel with the center of the cylinder bluff bodies. Separation angles of 85°, in particular, motivate early flow transition, producing additional stretching of the shear layer behind the cylinder bluff body and a larger near-wake flow formation. This condition matched the outcomes of a study of the transition of the boundary layer on a circular cylinder in the presence of trip, with the flow transition resulting in a broader near wake at Re = 10000 (Lee & Yang, 2013).

On the contrary, larger intensities of vortex shedding occur strongly behind the bluff bodies, creating increased mixing of the fluid flow and boosting the enhancement of turbulence flow. As the vortex shedding creation occurs in the infinite array arrangement, the shedding intensity movement is essentially repeated as in the looping system, leading the vortex shedding to alter as it crosses through the cylindrical bluff body again. A similar cycle of vortex shedding will occur if the Reynolds Number is increased while the angle of the trip wires is fixed at a given angle. In regard to formation length, the vortex sheds significantly longer downstream lengths as the trip wire angles applied to the cylinder bluff body increase. This is proportional to the fluid's viscosity, which correlates to the resistance to vortex formation. Since the arrangement uses a

https://doi.org/10.24191/jmeche.v22i3.3613

constant Reynolds Number, the viscosity of the fluid is substantially lower, permitting the vortex to shed strongly further downstream lengths after crossing the separation angles of the cylinder bluff body. The flow of viscous fluid occurs more quickly on the cylinder bluff body than on the channel wall, promoting a quicker rate of vortex shedding depending on the separation angles of the trip wires on the cylinder bluff bodies. This situation causes the fluid passing through the cylinder bluff bodies to have a constant viscosity, which tends to increase the formation length depending on the increment of the separation angles applied to the cylinder bluff bodies.

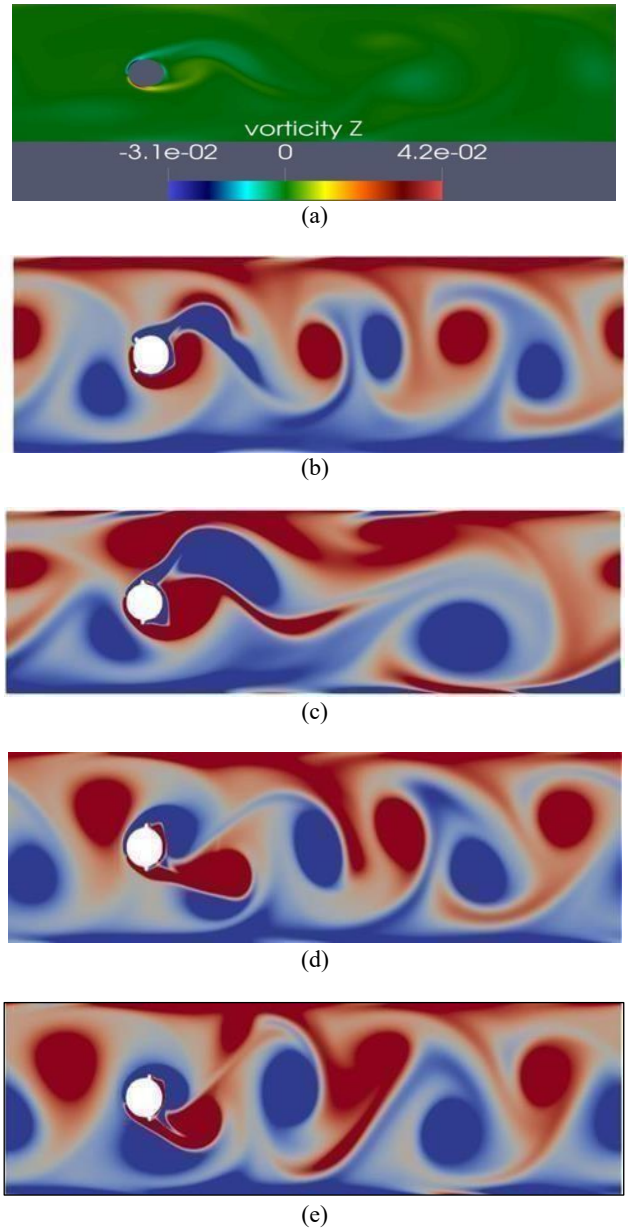

Fig. 4. Z-component vorticity contour for (a) without trip wire, trip wire with separation angles of (b) 45°, (c) 85°, (d) 95°, and (e) 105°.

https://doi.org/10.24191/jmeche.v22i3.3613

This result aligns with the findings of Ishihara & Li (2020), who studied the suppression of vortex-induced vibrations in a circular cylinder using helical wires and visualized the wake vorticity patterns. For the unwired cylinder, two pairs of vortices appeared in the initial branch and persisted downstream. In contrast, for the wired cylinder, the vortices were disrupted and intensified by the wires. The helical wires also controlled the separation points at various cross-sections and significantly influenced the wake width. A turbulence wire significantly affects flow characteristics and drag reduction, with its effectiveness highly dependent on the installation location, whereby a maximum drag reduction of up to 75% was observed at air velocities of 15 m/s and 25 m/s when applied to an elliptic cylinder positioned at angles of 23.7° and 40.9° relative to the stagnation point (Yadegari & Khoshnevis, 2021). Surface geometry manipulation can also alter the vorticity contour, as confirmed by wind tunnel tests on a circular cylinder fitted with 12 spiral protuberances (Dao et al., 2023). The results showed a 33% reduction in drag and suppression of Kármán vortex shedding within a Reynolds number range of 13,000 to 31,000, and this drag reduction became more pronounced with increasing Reynolds numbers and contributed to delaying flow separation points.

Velocity Flow Field

Relationship between the velocity magnitude and the condition of the vorticity shedding frequency after passing the cylinder bluff bodies, as illustrated in Fig 4 and Fig 5, is used to investigate the heat transfer generation in the flow channel. In this domain arrangement, the enhancement of the convective heat transfer is achieved using the passive techniques by employing the trip wires, which are symmetrically located at the circumferential area of the cylinder bluff body. The mixing of the flow is intended to be greater in order to improve heat transfer generation. Four trip wires of varying diameters were installed on a 20 mm circular cylinder at angular positions of $\theta = \pm 40°$ and $\pm 140°$, and tested under flow velocities of 2.85 m/s, 10 m/s, and 20 m/s. The results show that the vortex patterns are highly sensitive to the trip wire placement, with smaller trip wire diameters leading to a shorter shear layer. Velocity contours also exhibited turbulent patterns, particularly at the $\theta = \pm 140°$ positions, consistent with the observations presented in Fig 5 (Mansouri et al., 2023). It is assumed that the velocity of fluid is zero (no-slip boundary condition) at the wall of the flow channel is applied. As a consequence, heat is transferred from the solid surface to the fluid layer close to it by pure conduction. The production of convection heat transfer varies along the flow direction.

According to Fig 5(b), velocity magnitude decreases significantly after crossing the cylinder bluff bodies, resulting in a reduced improvement in convective heat transfer. The velocity magnitude gradually declines near the channel's end, resulting in lower heat transfer generation. By referring to the vorticity contour on Fig 5(b), the vortex sheds are less vigorous compared to other separation angles in which indicating lesser mixing of flow to enhance the heat transfer process to occur. Nevertheless, the enhancement of convective heat transfer is slightly larger at specific separation angles due to the higher magnitude of velocity created after passing through the cylinder bluff bodies. In contrast to the effect of velocity magnitude shown on the separation angles of Fig 5(c), Fig 5(d) and Fig 5(e) explicitly show that the changing in phase of the velocity magnitude is relatively higher after passing the cylinder bluff bodies, where the position of the separation angle causes the flow to slightly move alternately toward the wall. Thus, the enhancement of convective heat transfer is increasing gradually. In the case of vortex shedding, the relationship is based mostly on the intensity of the vortex shedding behind the cylinder bluff bodies. In theory, increasing the intensity of vortex shedding will result in an increase in the percentage improvement in the flow's Nusselt number. Relating to Fig 4(d) and Fig 4(e), the vortex shedding intensity is significantly higher, indicating stronger flow mixing. Due to the location of the separation angles on the cylinder bluff bodies, there is greater mixing of the flow behind the bodies, which causes the flow to transfer heat more vigorously. This has an effect on the distribution of temperatures behind the bodies and causes substantial alterations in the vertical direction along the desired distance beyond the cylinder bluff bodies.

https://doi.org/10.24191/jmeche.v22i3.3613

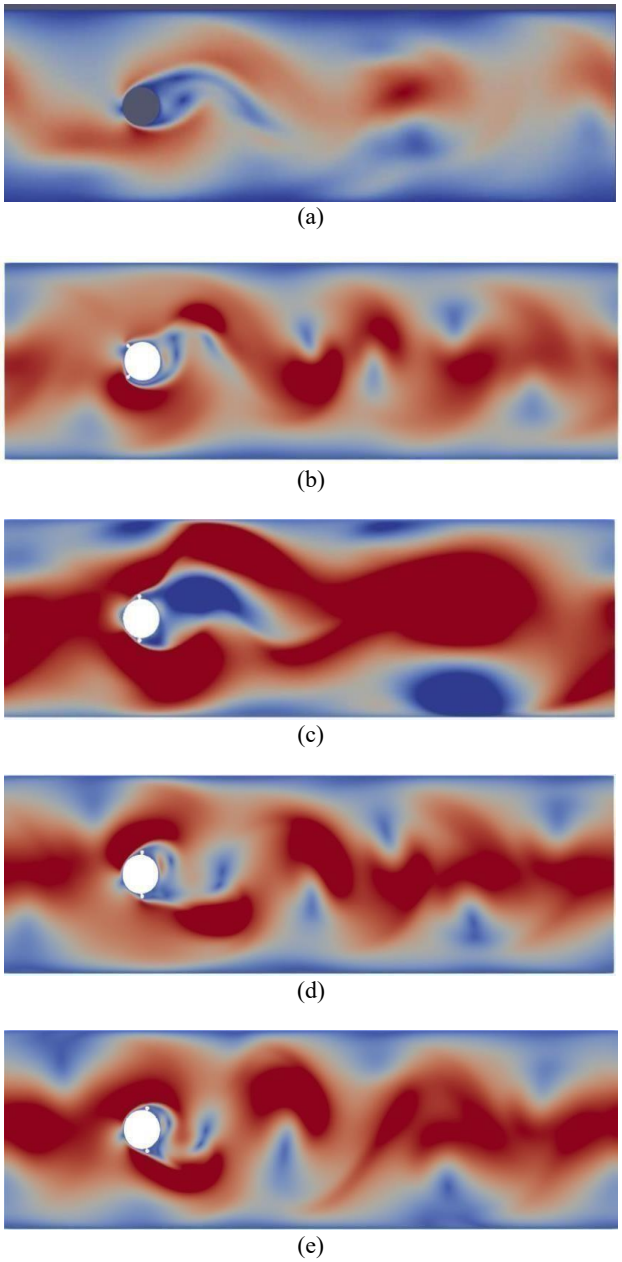

Fig. 5. Contour plot of velocity magnitude for (a) without trip wire, trip wire with separation angles of (b) 45°, (c) 85° (d) 95°, and (e) 105°

Fast Fourier Transformation (FFT) calculation has been tabulated, which gives information about the dominant frequency at the location on the cylinder surface and indicates whether our flow calculation captured the flow field in a timely accurate manner. The result shows the highest peak occurs at a separation angle of 85^0, indicating that early transition of the vorticity has taken place at this angle.

https://doi.org/10.24191/jmeche.v22i3.3613

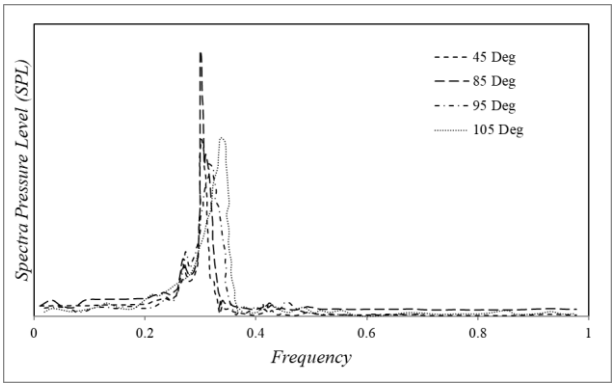

Fig. 6. Shedding frequency at the surface of cylinder.

CONCLUSION

The trip wires were split symmetrically with separation angles varying from 45° to 135°. The findings showed that the inclusion of trip wires on the cylinder bluff body greatly promotes an early boundary layer transition, leading to changes in vortex shedding size and frequency. Also shown that the vortex sheds significantly longer downstream distances with the rise of the trip wires angles applied to the cylinder bluff body. This is proportional to the fluid's viscosity, which correlates to the resistance to vortex formation. The results revealed that at the separation angle of 85°, the vortex shedding condition shows significant variations in shedding intensity, with relatively less vortex shedding formation owing to the position of the separation angles being almost parallel with the center of the cylinder bluff bodies. The separation angles of 85° promote early transition of the flow, creating additional stretching of the shear layer behind the cylinder bluff body, leading to a wider near wake of flow formation, which leads to a higher intensity of vortex shedding, which strongly develops behind the bluff bodies, causing greater mixing of the fluid flow and promoting the enhancement of turbulence flow.

The inclusion of trip wires on the cylinder bluff body alters the wake formation downstream of the cylinder bluff body, which varies for each case, boosting turbulence flow in the channel. The wake region around the flow transition indicated fluctuations in flow stability and growth under the infinite array design, allowing for enhanced turbulence flow as anticipated for the current study. The outcomes demonstrated that the wake region exhibited chaotic mixing of flow at separation angles practically parallel to the center of the cylinder bluff body, indicating a broader near wake of flow formation. When the separation angles are farther away from the parallel center of the cylinder bluff body, the concentration of flow mixing is found to be smaller. In all of the instances studied in this work, the turbulence state gradually decreases near the channel's end, resulting in less violent mixing between the flows moving through the channel's exit.

ACKNOWLEDGEMENTS/ FUNDING

Faculty of Mechanical Engineering Universiti Teknologi MARA for provide facilities for master's degree programs, MSc in Mechanical Engineering (Mixed Mode).

https://doi.org/10.24191/jmeche.v22i3.3613

CONFLICT OF INTEREST STATEMENT

The authors agree that this research was conducted in the absence of any self-benefits, commercial or financial conflicts and declare the absence of conflicting interests with the funders.

AUTHORS' CONTRIBUTIONS

The authors confirm their contribution to the paper as follows: **study conception and preliminary study**: Mohd Hafiz Mohd Noh, Ahmad Hussein Abdul Hamid; **data collection and simulation**: Mohd Ridzuan Sejon; **analysis and interpretation of results**: Mohd Hafiz Mohd Noh, Ahmad Hussein Abdul Hamid, Waseem Ahmed Rzaij Faraj; **draft manuscript preparation**: Mohd Hafiz Mohd Noh, Waseem Ahmed Rzaij Faraj. All authors reviewed the results and approved the final version of the manuscript.

REFERENCE

Abramzon, B., & Elata, C. (1984). Unsteady heat transfer from a single sphere in Stokes flow. International Journal of Heat and Mass Transfer, 27(5), 687-695.

Behara, S., & Mittal, S. (2011). Transition of the boundary layer on a circular cylinder in the presence of a trip. Journal of Fluids and Structures, 27(5-6), 702-715.

Bhattacharyya, S., Khan, A. I., Maity, D. K., Pradhan, S., & Bera, A. (2017). Hydrodynamics and heat transfer of turbulent flow around a rhombus cylinder. Chemical Engineering Transaction, 62, 373–378.

Chambré, P. L., & Young, J. D. (1958). On the diffusion of a chemically reactive species in a laminar boundary layer flow. Physics of Fluids, 1(1), 48-54.

Chopra, G., & Mittal, S. (2022). The effect of trip wire on transition of boundary layer on a cylinder. Physics of Fluids 34, 054103.

Dao, T., Matsumiya, H., Noguchi, K., Xu, R., Marey, O., & Yagi, T. (2023). Drag reduction of a cylinder by using spiral protuberances to generate three-dimensional surface flow. Journal of Wind Engineering and Industrial Aerodynamics, 241, 105550.

Dhiman, A., & Shyam, R. (2011). Unsteady heat transfer from an equilateral triangular cylinder in the unconfined flow regime. ISRN Mechanical Engineering, 2011(1), 932738.

Duan, G., Laima, S., Chen, W., & Li, H. (2021). Effects of leading-edge separation on the vortex-induced vibration of an elongated bluff body. Journal of Wind Engineering and Industrial Aerodynamics, 209, 104500.

Ishihara, T., & Li, T. (2020). Numerical study on suppression of vortex-induced vibration of circular cylinder by helical wires. Journal of Wind Engineering and Industrial Aerodynamics, 197, 104081.

Konopliv, N., & Sparrow, E. M. (1970). Transient heat conduction in nonhomogeneous spherical systems. Heat and Mass Transfer, 3(4), 197-210.

Kravets, B., Rosemann, T., Reinecke, S. R., & Kruggel-Emden, H. (2019). A new drag force and heat transfer correlation derived from direct numerical LBM-simulations of flow through particle packings. Powder Technology, 345, 438-456.

https://doi.org/10.24191/jmeche.v22i3.3613

Lee, K., & Yang, K. S. (2013). Flow instability in obstructed channel flow. Computers and Fluids, 84, 301-314.

Lekkala, M. R., Latheef, M., Jung, J. H., Coraddu, A., Zhu, H., Srinil, N., Lee, B. H., & Kim, D. K. (2022). Recent advances in understanding the flow over bluff bodies with different geometries at moderate Reynolds numbers. Ocean Engineering, 261, 111611.

Luo, X., Zhang, W., Dong, H., Thakur, A. K., Yang, B., & Zhao, W. (2021). Numerical analysis of heat transfer enhancement of fluid past an oscillating circular cylinder in laminar flow regime. Progress in Nuclear Energy, 139, 103853.

Lysenko, D. A., Donskov, M., & Ertesvag, I. S. (2023). Large-eddy simulations of the flow past a bluff-body with active flow control based on trapped vortex cells at Re = 50000. Ocean Engineering, 280, 114496.

Mansouri, Z., Yadegari, M., & Bak Khoshnevis, A. (2023). Numerical investigation of the effects of installing four trip wires with different diameters on the mean and fluctuation velocities and characteristics of the wake around the circular cylinder. Journal of the Brazilian Society of Mechanical Sciences and Engineering, 45, 459.

Murmu, S. C., Bhattacharyya, S., Chattopadhyay, H., & Biswas, R. (2020). Analysis of heat transfer around bluff bodies with variable inlet turbulent intensity: A numerical simulation. International Communications in Heat and Mass Transfer, 117, 104779.

Nguyen, H. D., Paik, S., & Chung, J. N. (1993). Unsteady mixed convection heat transfers from a solid sphere: The conjugate problem. International Journal of Heat and Mass Transfer, 36(18), 4443-4453.

Romkes, S. J. P., Dautzenberg, F. M., Bleek, C. M. V. D., & Calis, H. P. A. (2003). CFD modelling and experimental validation of particle-to-fluid mass and heat transfer in a packed bed at very low channel to particle diameter ratio. Chemical Engineering Journal, 96(1-3), 3-13.

Roshko, A. (1955). On the wake and drag of bluff bodies. Journal of the Aeronautical Sciences, 22(2), 124–32.

Sahin, B., Manay, E., & Ozceyhan, V. (2013). Overall heat transfer enhancement of triangular obstacles. International Journal of Automotive and Mechanical Engineering, 8, 1278–1291.

Sareen, A., Hourigan, K., & Thompson, M. C. (2024). Passive control of flow-induced vibration of a sphere using a trip wire. Journal of Fluids and Structures, 124, 104052.

Vyas, A., Yadav, A., & Srivastava, A. (2020). Flow and heat transfer measurements in the laminar wake region of semi-circular cylinder embedded within a rectangular channel. International Communications in Heat and Mass Transfer, 116, 104692.

Yadegari, M., & Khoshnevis, A. B. (2021). Numerical and experimental study of characteristics of the wake produced behind an elliptic cylinder with trip wires. Iranian Journal of Science and Technology, Transactions of Mechanical Engineering, 45(1), 265-285.

https://doi.org/10.24191/jmeche.v22i3.3613